Electronic Supplementary Material (ESI) for RSC Advances.

Supporting Information

Novel 2-Substituted-Quinoxaline analogs with Potential Antiproliferative Activity against breast cancer: insights into cell cycle arrest, Topoisomerase II, and EGFR activity

Manar G. Salem [1], Sara A. Abu El-ata [2], Elsherbiny H. Elsayed [2], Suraj N. Mali [3], Hussah Abdullah Alshwyeh [4,5], Ghassan Almaimani [6], Riyad A. Almaimani [7], Hussain A. Almasmoum [8], Najla Altwaijry [9], Ebtesam Al-Olayan [10], Essa M. Saied [11,12]*, Mohamed F. Youssef [13,*]

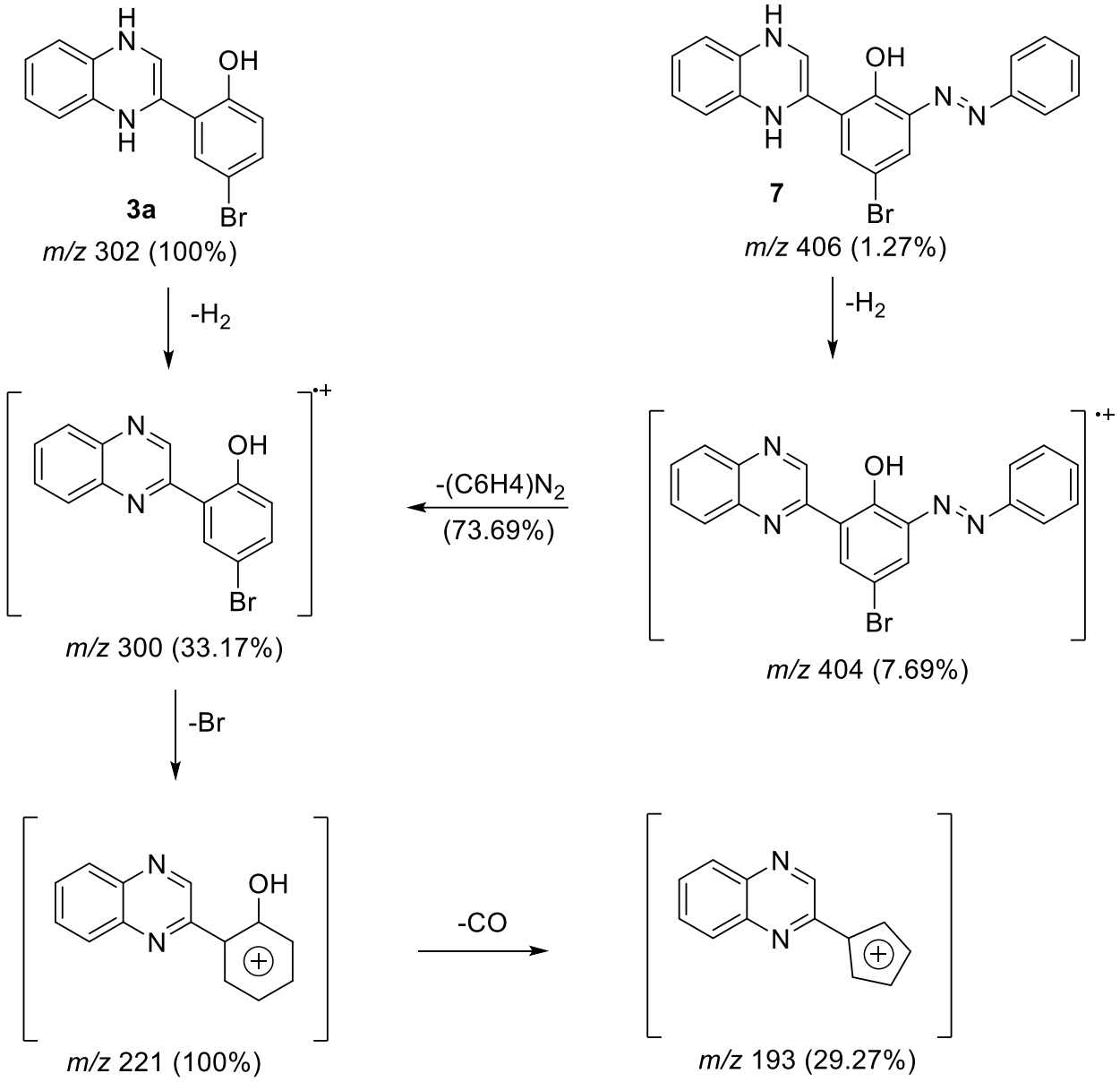

Scheme S1: Mass fragmentation pattern for compounds **3a**, and **7**.

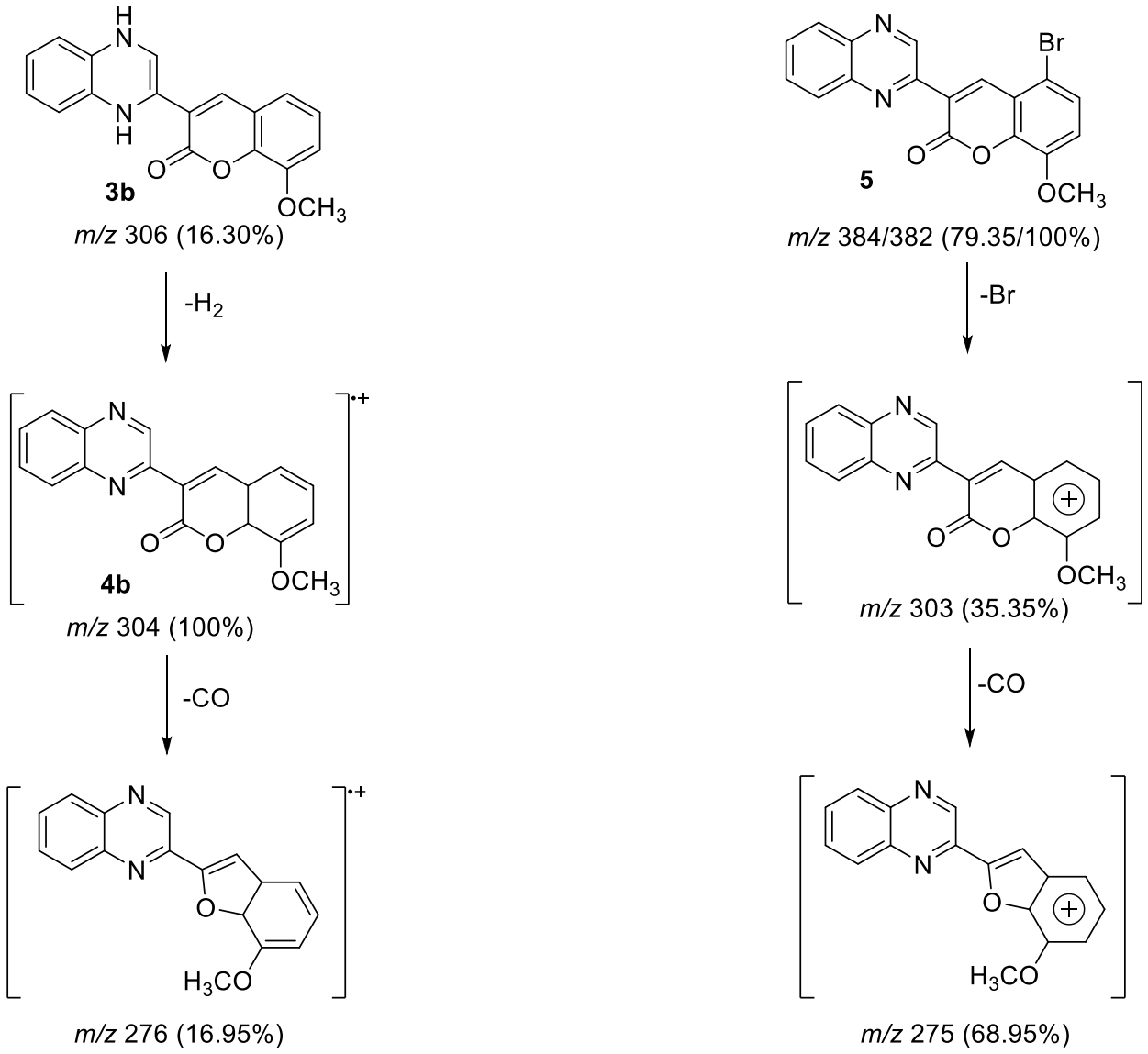

Scheme S2: Mass fragmentation pattern for compounds **3b**, **4b**, and **5**.

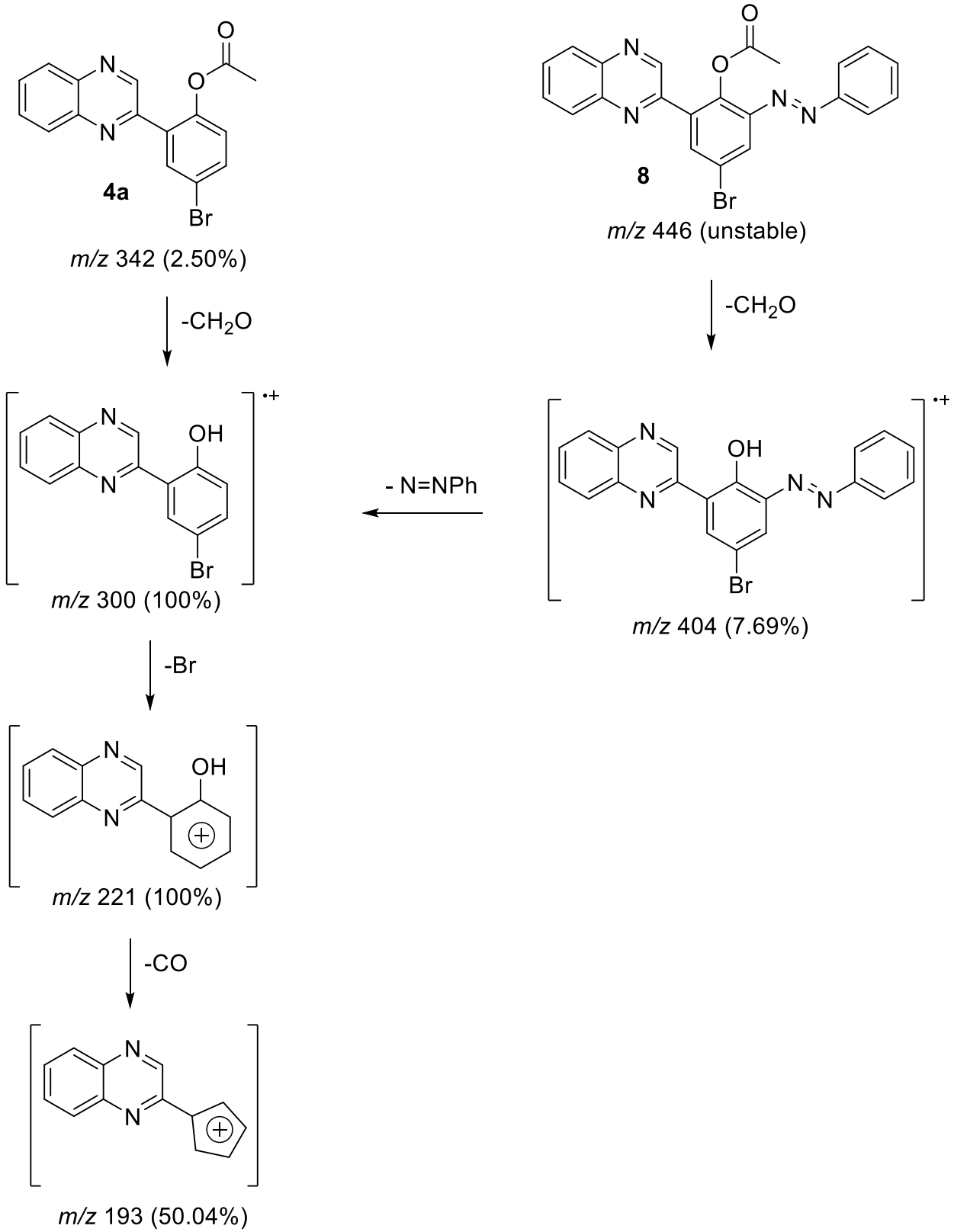

Scheme S3: Mass fragmentation pattern for compounds **4a**, and **8**.

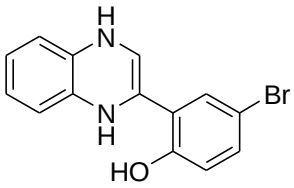

Compound **3a**

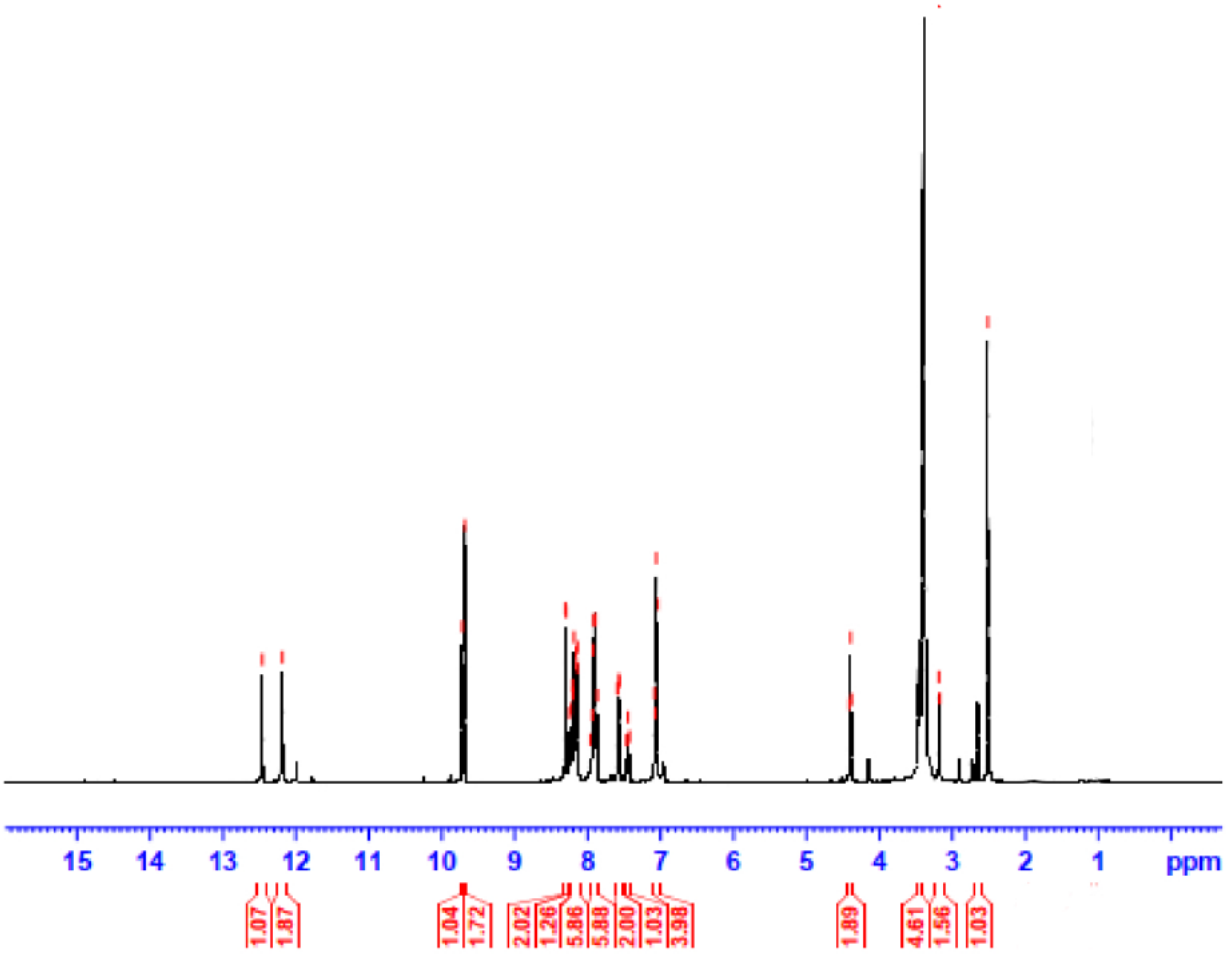

Figure 1a: ^{1}H NMR Spectrum of compound **3a**

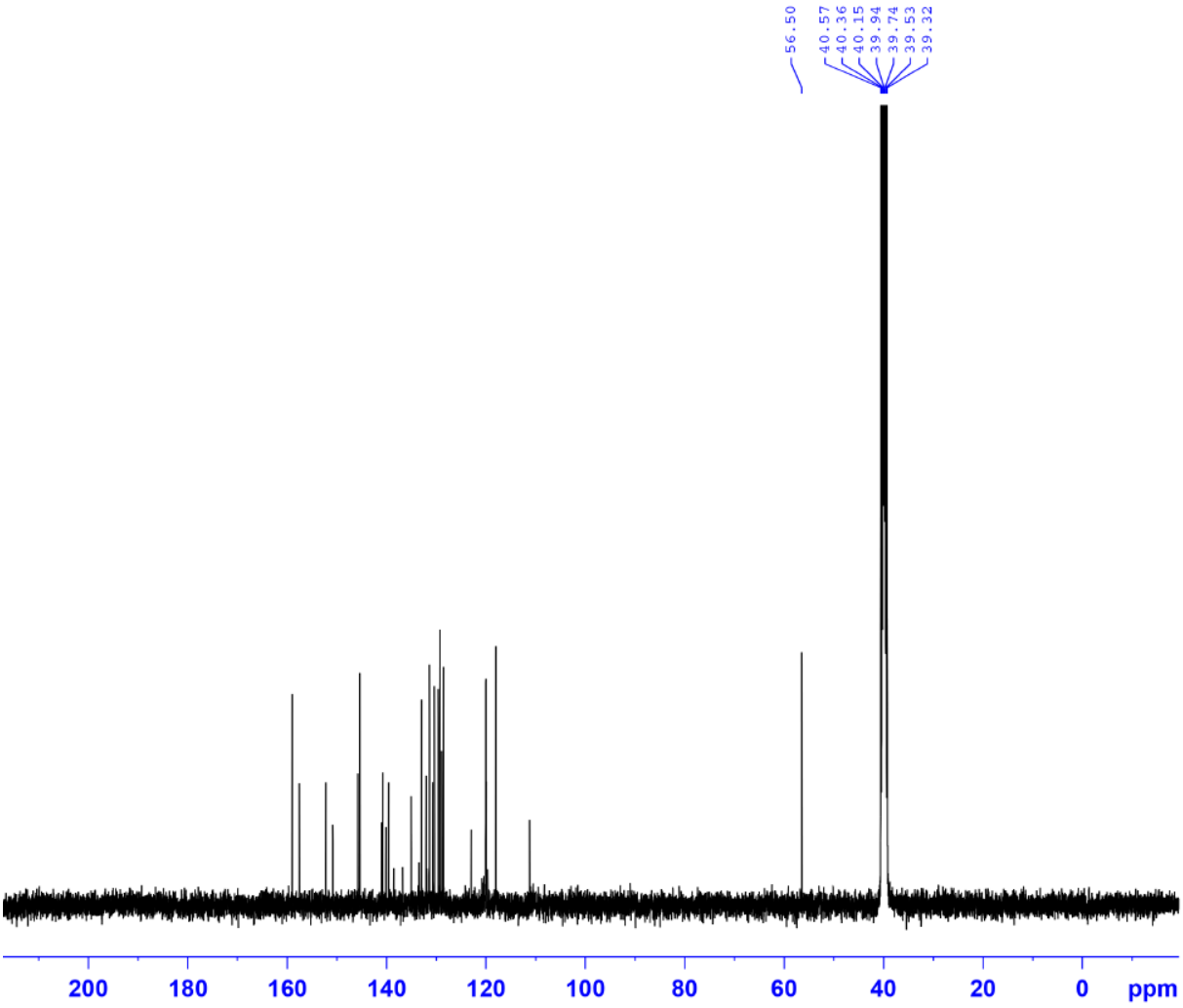

Figure 1b: ^{13}C NMR Spectrum of compound **3a**

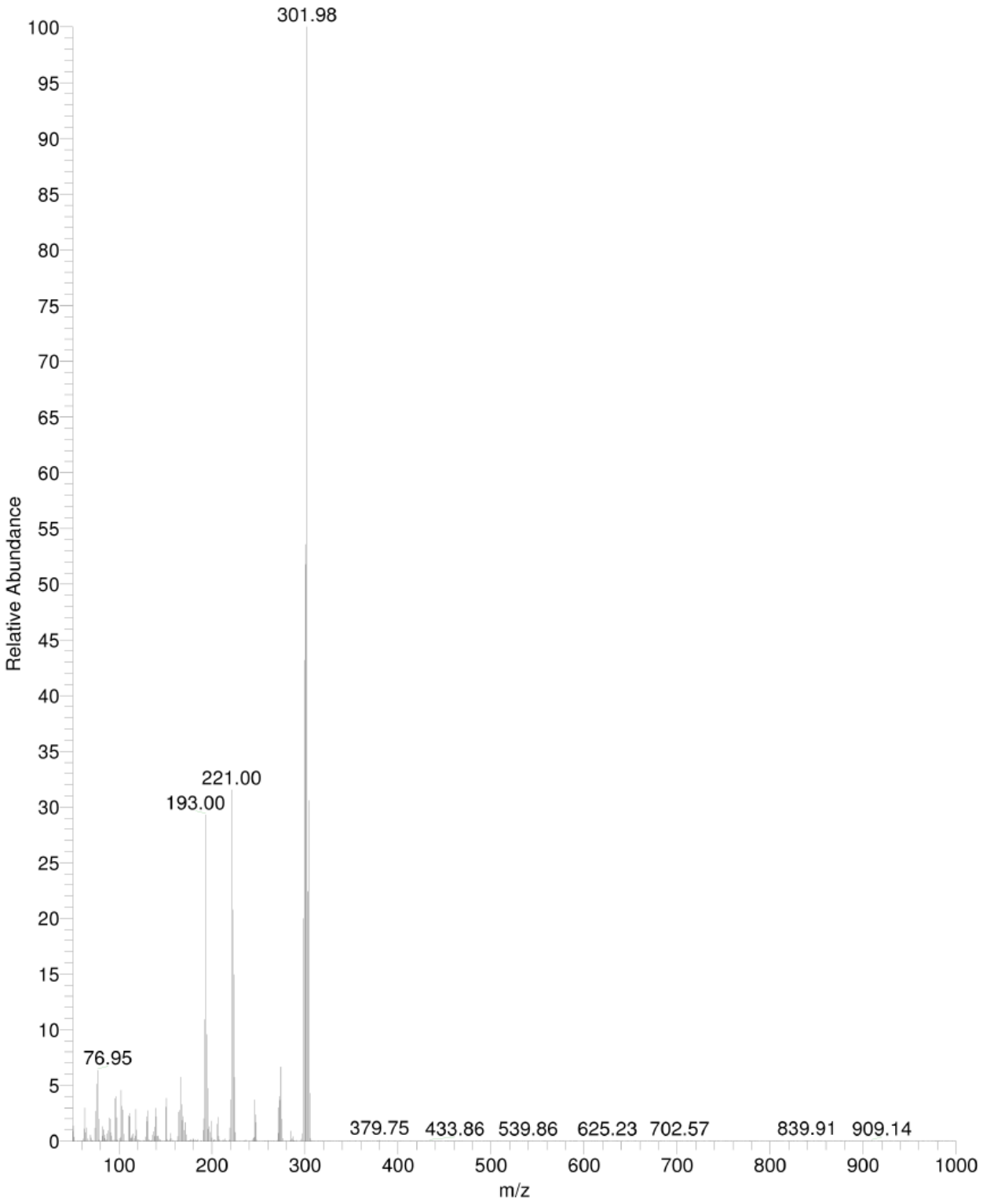

Figure 1c: Mass Spectrum of compound **3a**

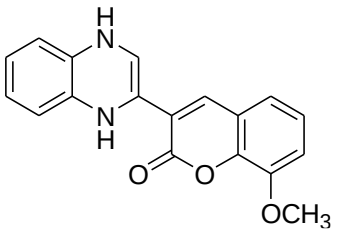

Compound **3b**

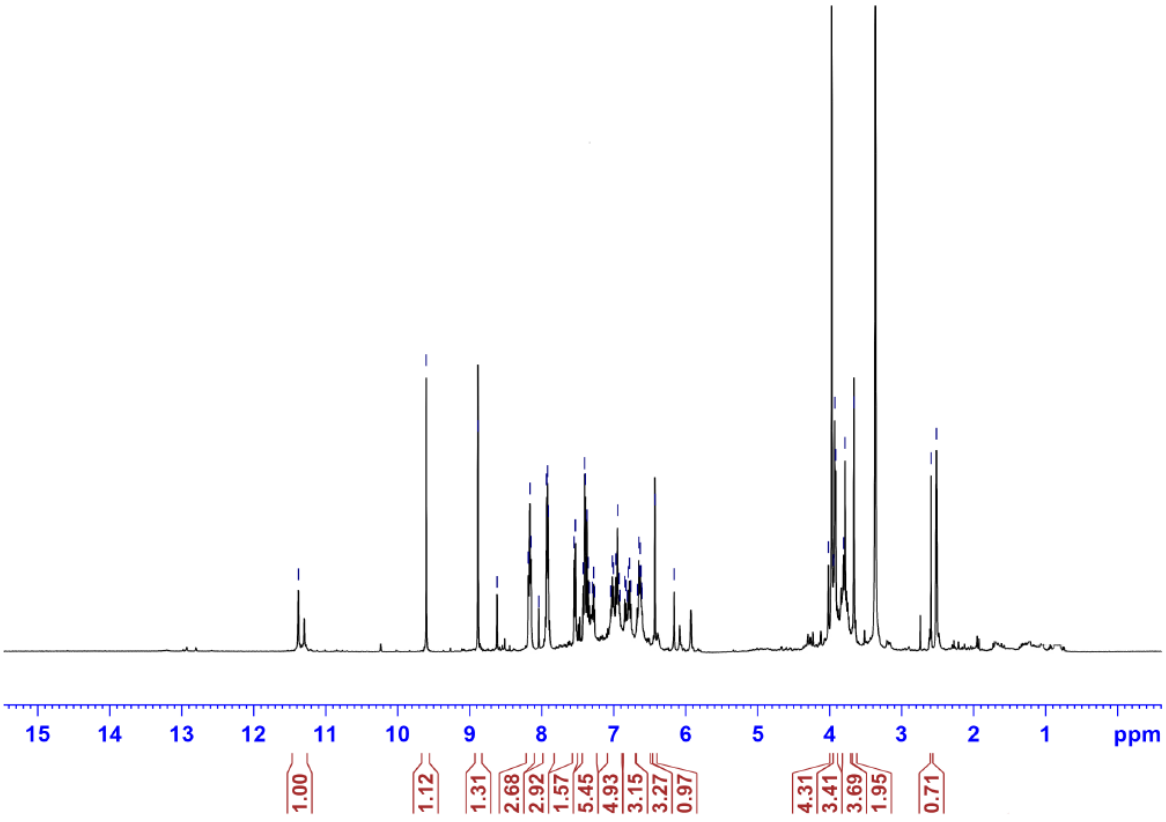

Figure 2a: ^{1}H NMR Spectrum of compound **3b**

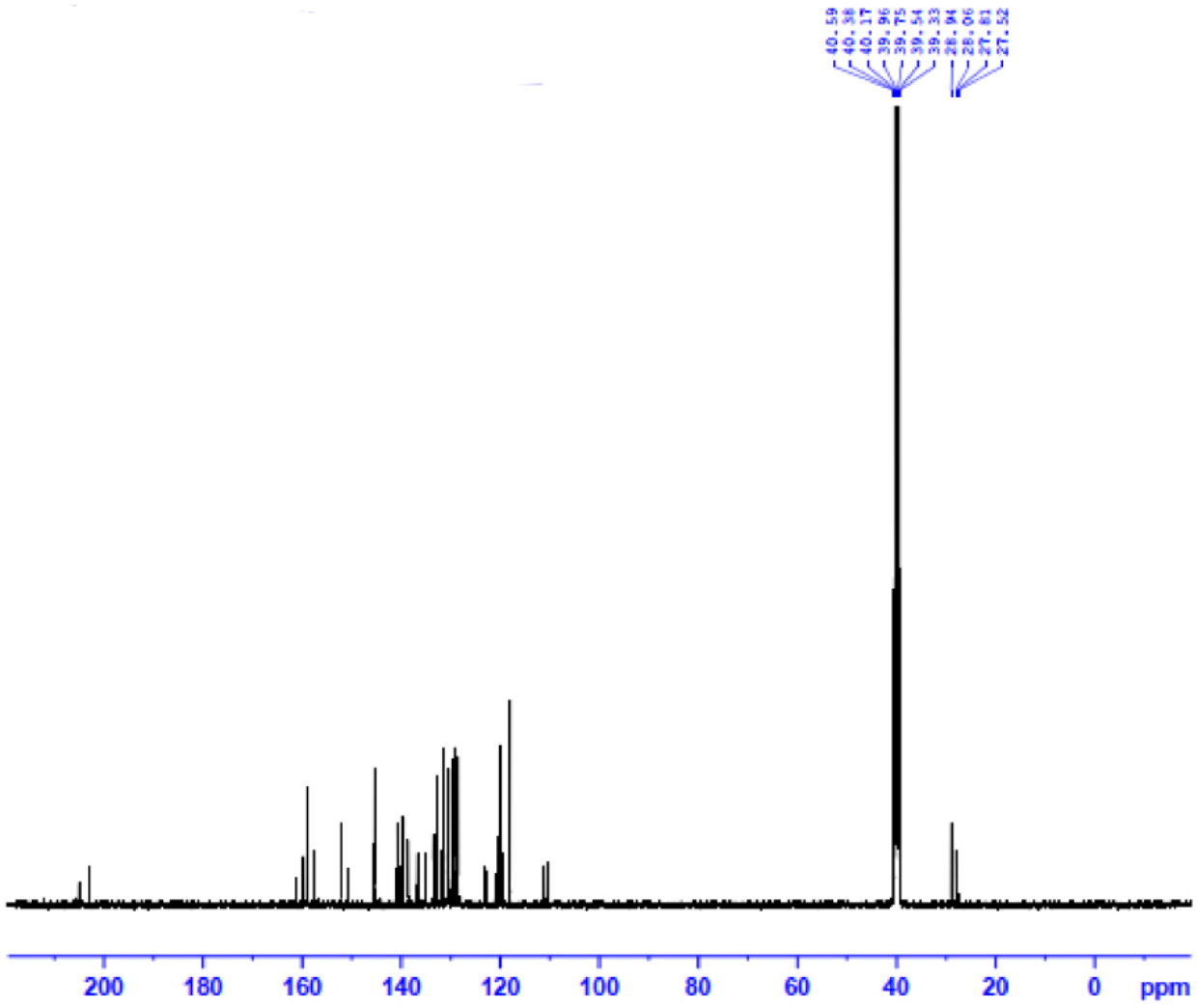

Figure 2b: ^{13}C NMR Spectrum of compound **3b**

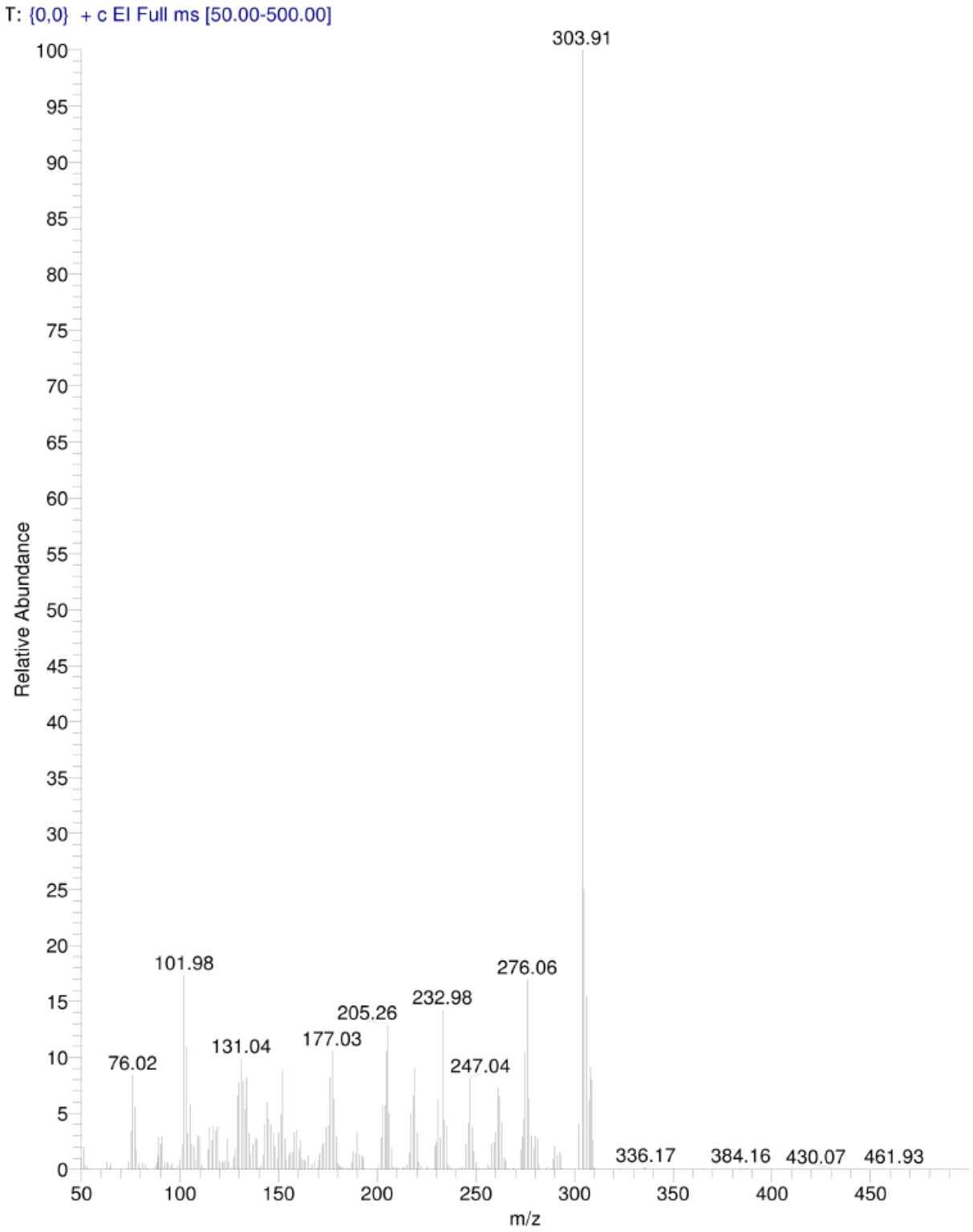

Figure 2c: Mass Spectrum of compound **3b**

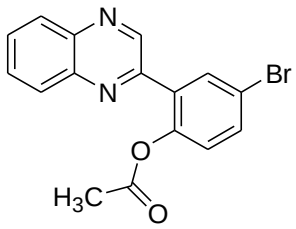

Compound **4a**

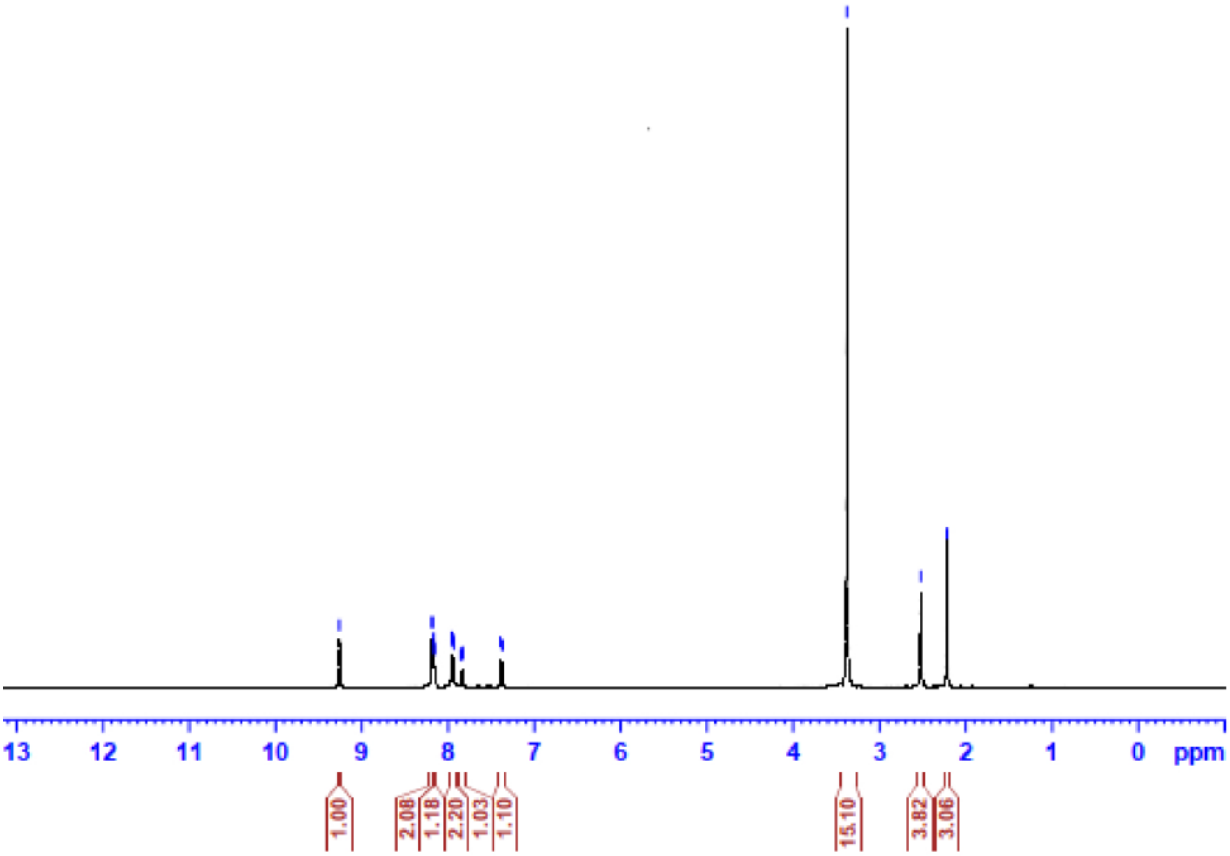

Figure 3a: ^{1}H NMR Spectrum of compound **4a**

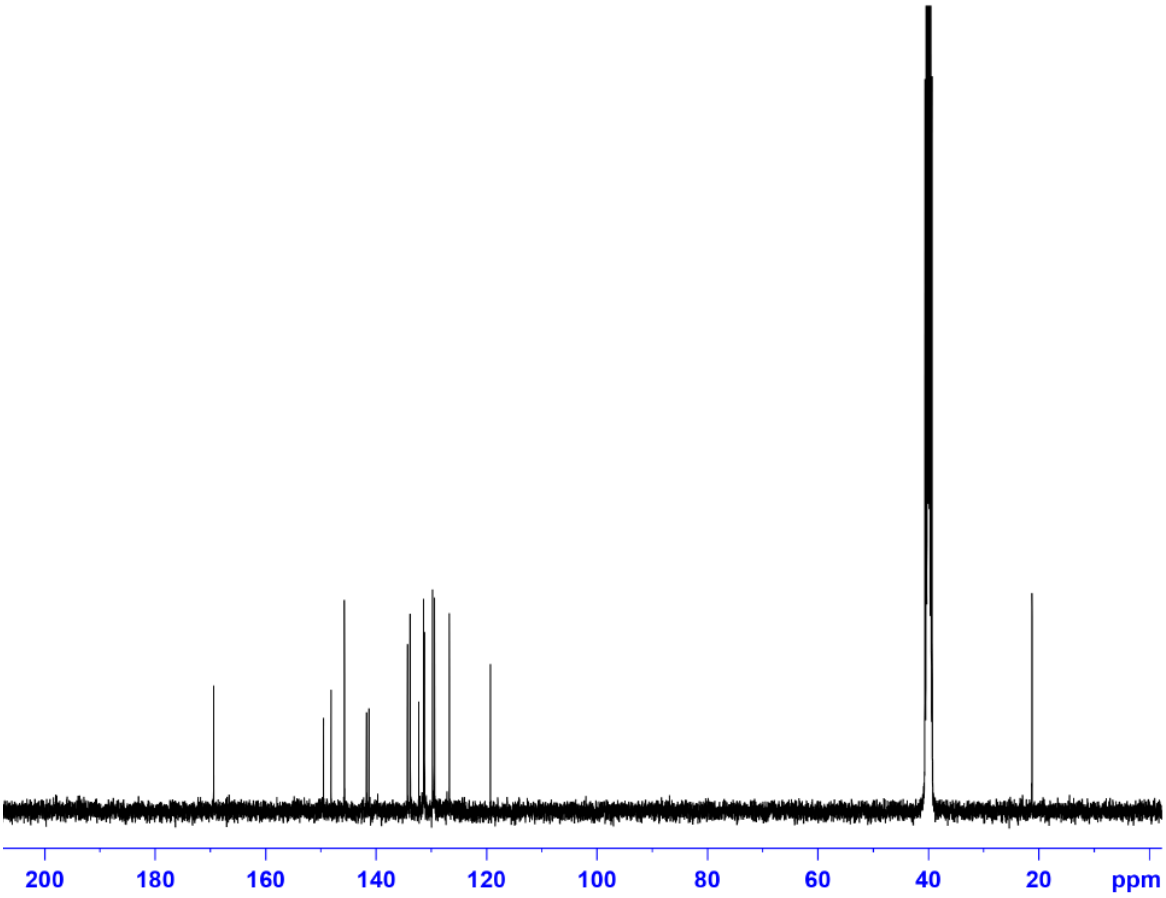

Figure 3b: ^{13}C NMR Spectrum of compound **4a**

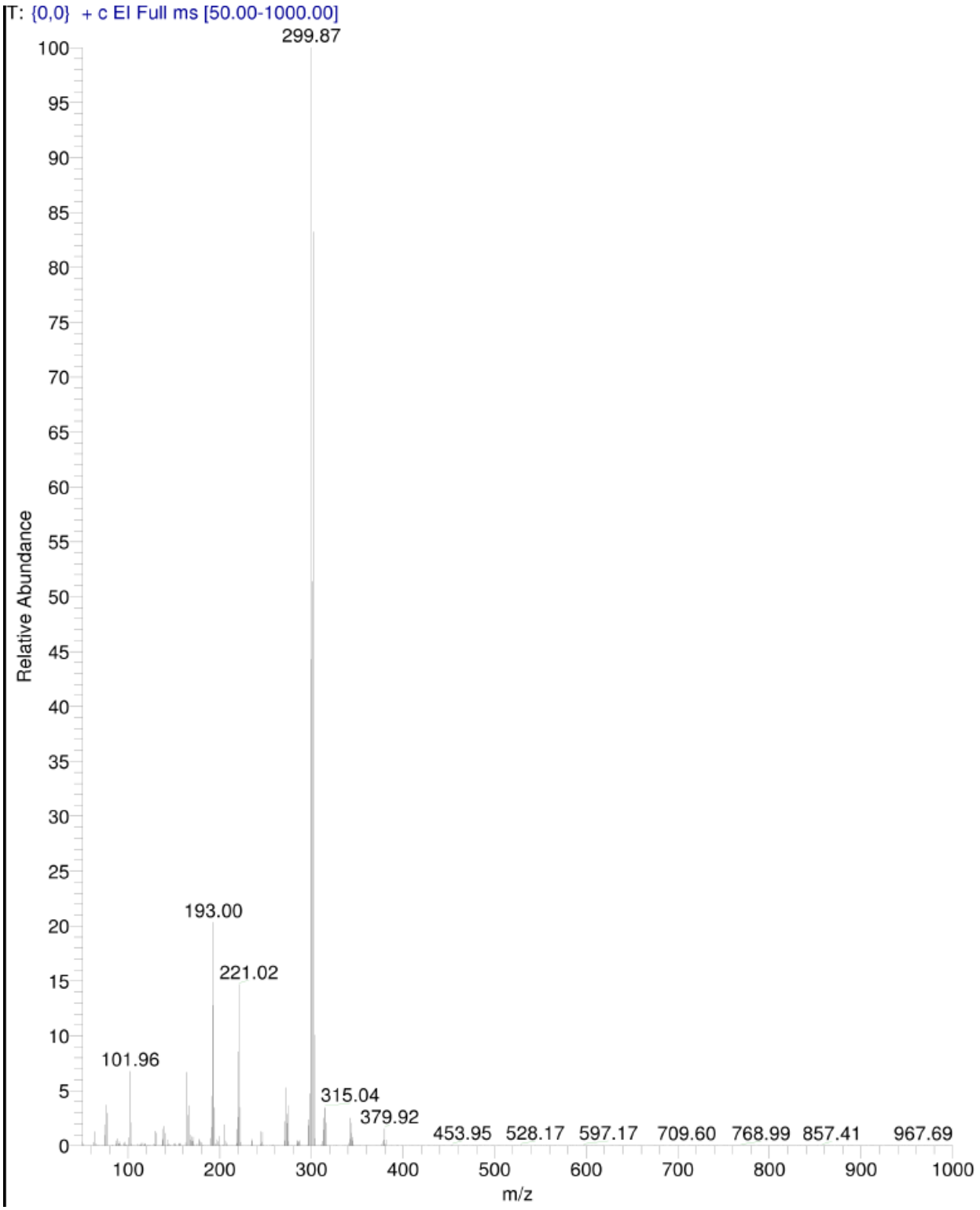

Figure 3c: Mass Spectrum of compound **4a**

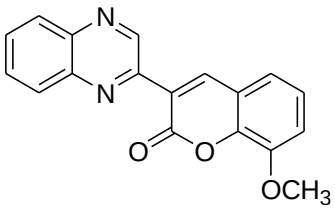

Compound **4b**

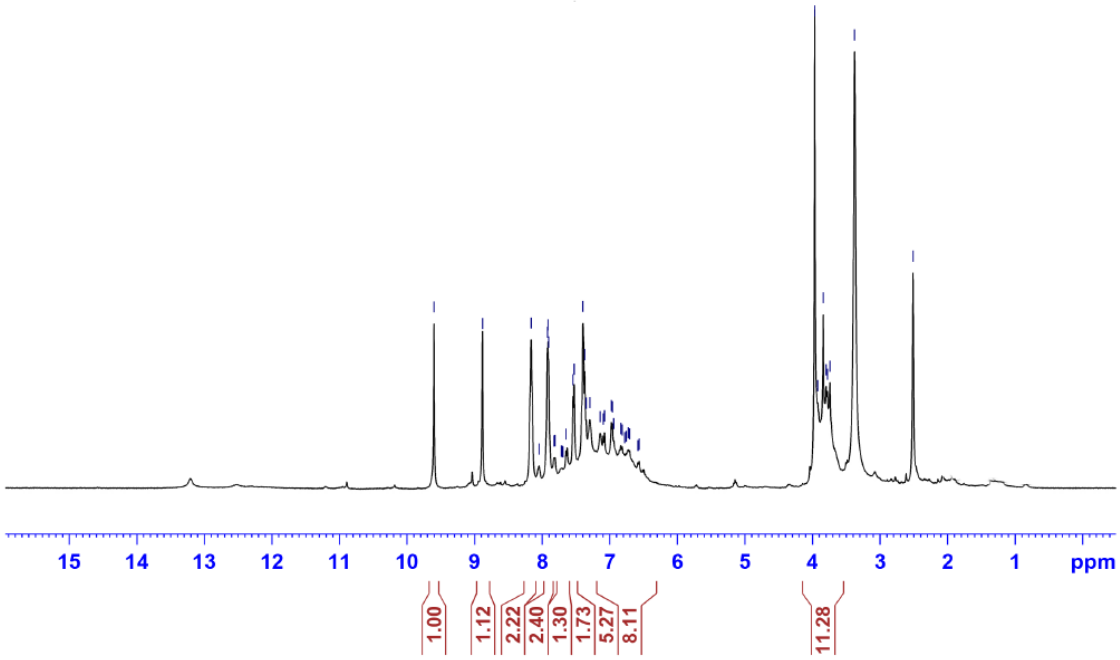

Figure 4a: ^{1}H NMR Spectrum of compound **4b**

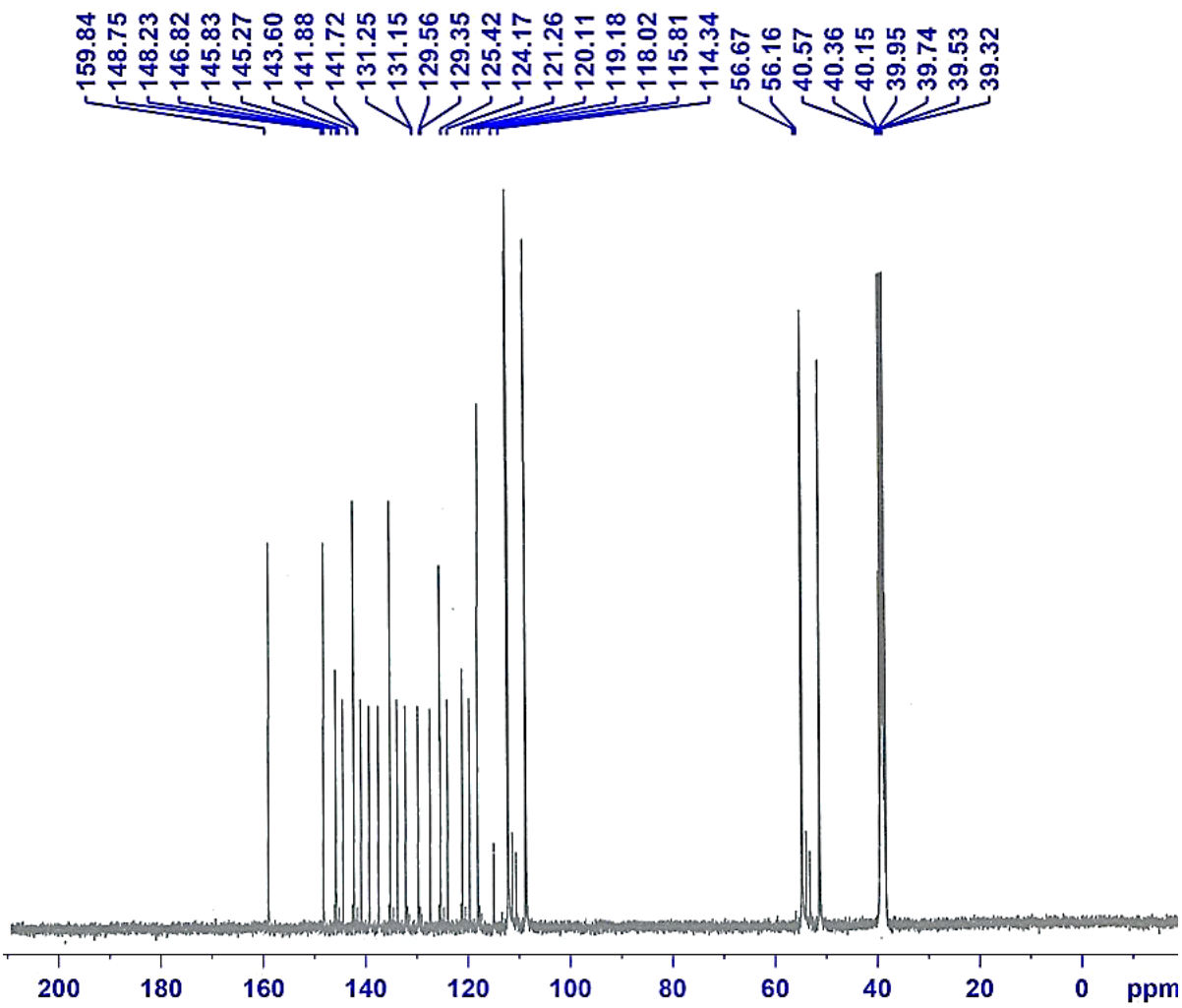

Figure 4b: ^{13}C NMR Spectrum of compound **4b**

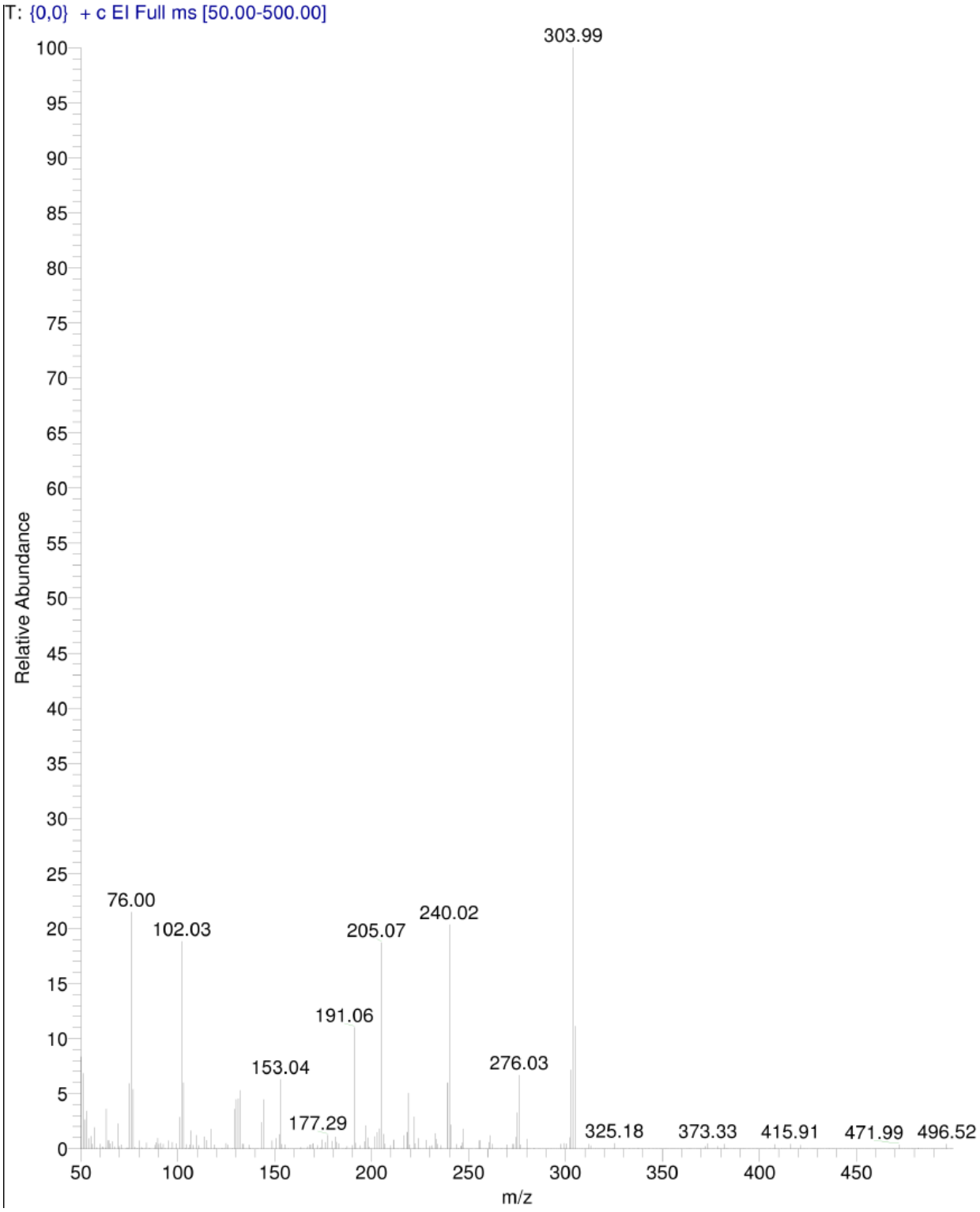

Figure 4c: Mass Spectrum of compound **4b**

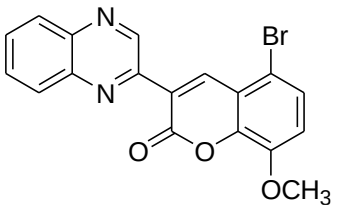

Compound **5**

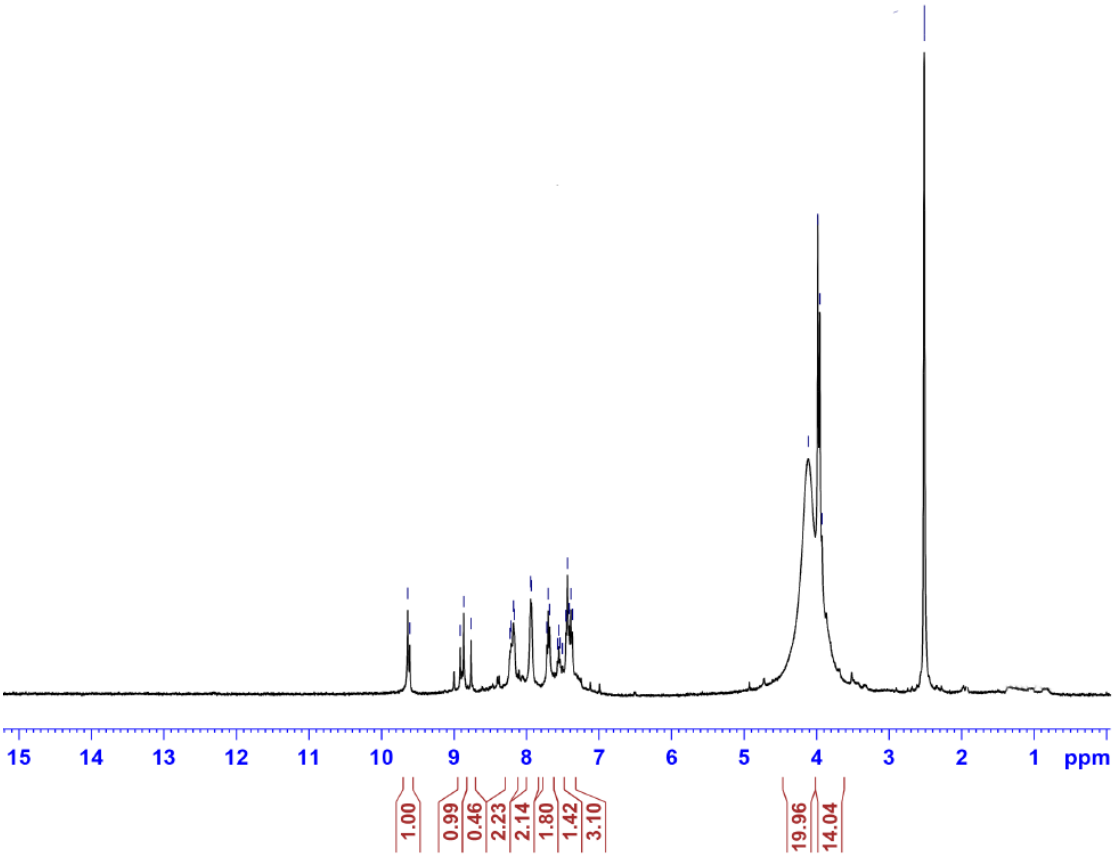

Figure 5a: ^{1}H NMR Spectrum of compound **5**

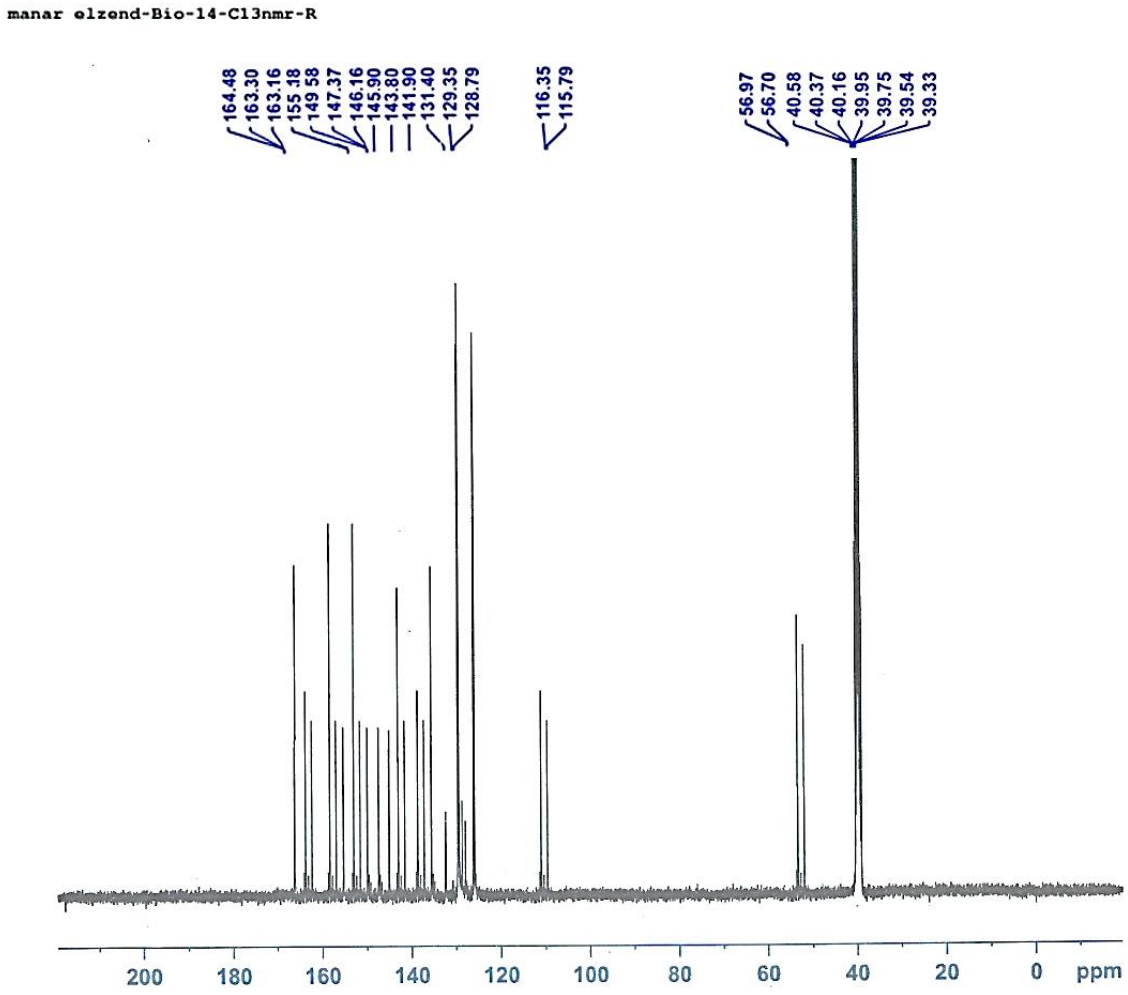

Figure 5b: ^{13}C NMR Spectrum of compound **5**

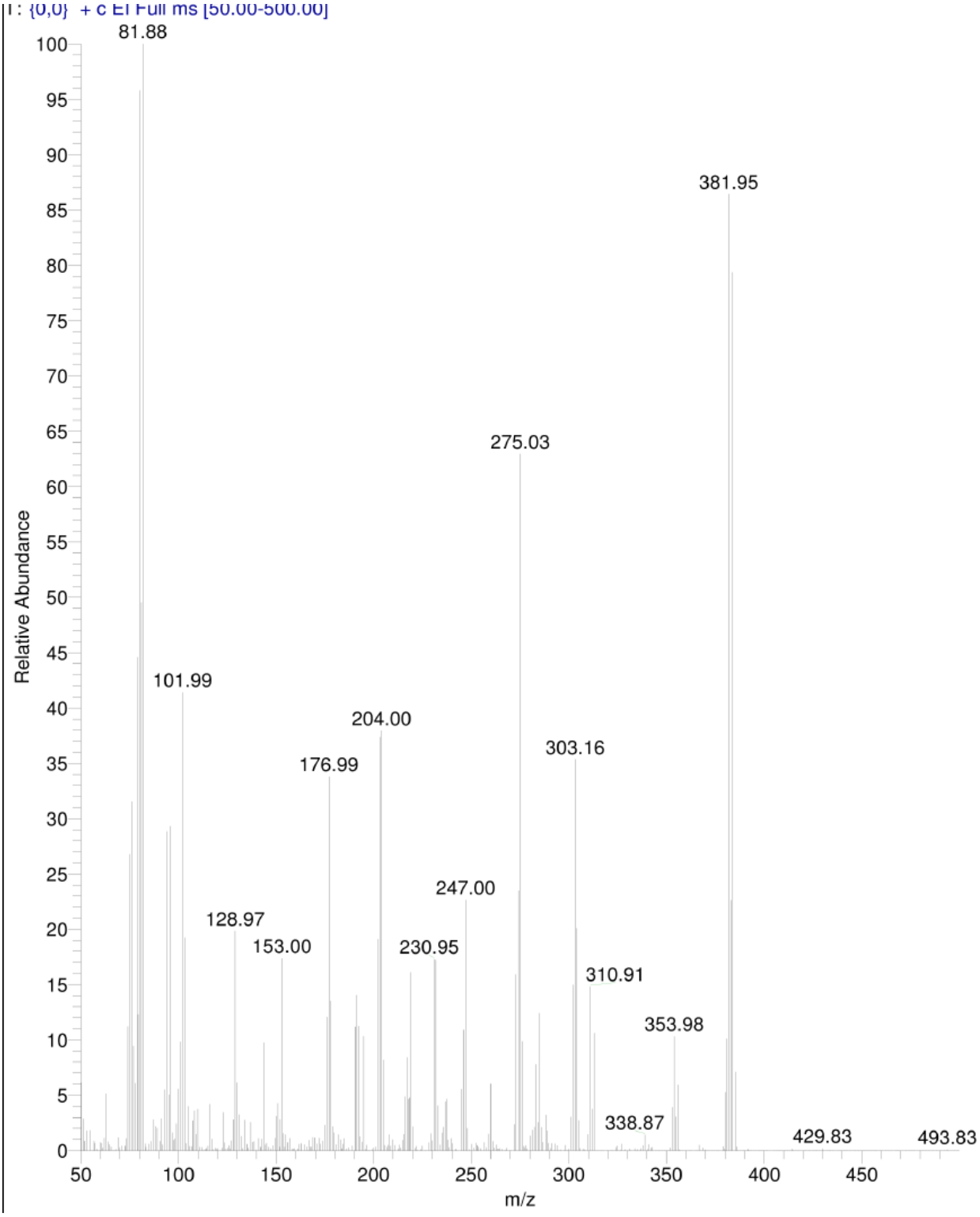

Figure 5c: Mass Spectrum of compound **5**

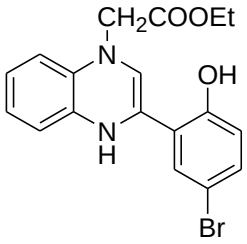

Compound **6**

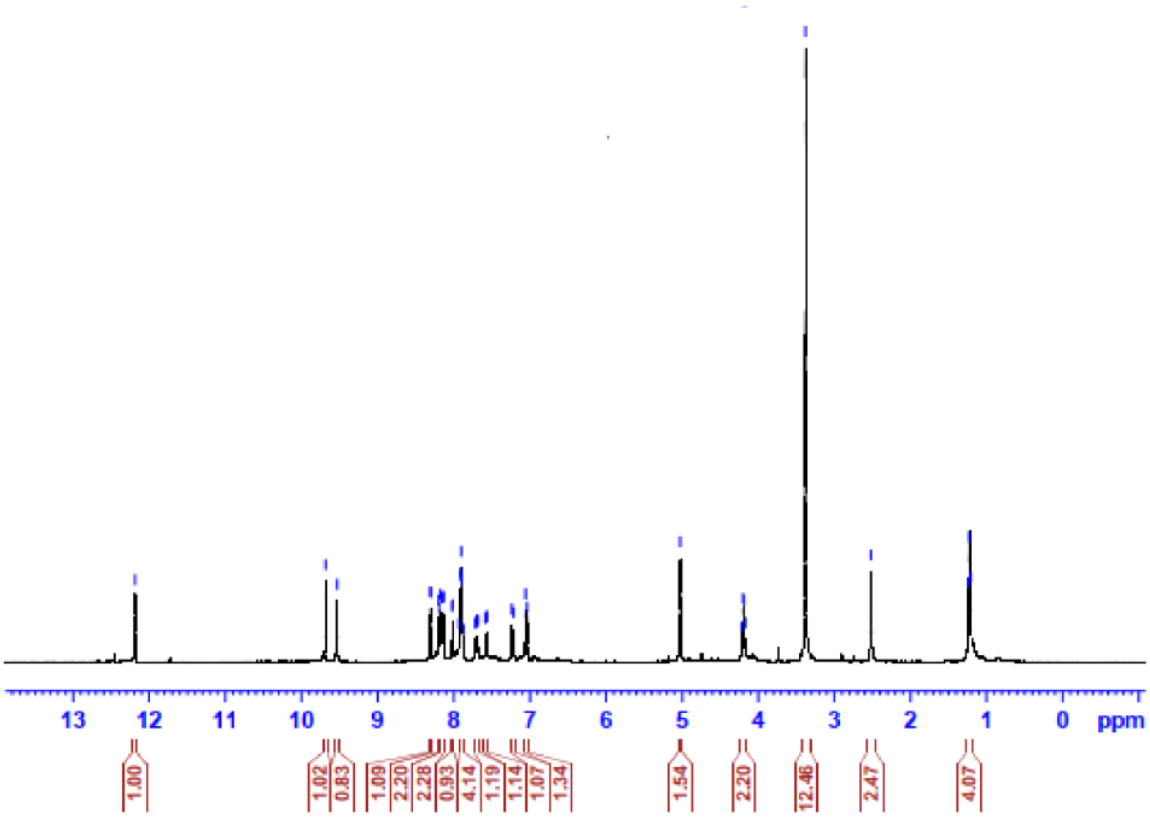

Figure 6a: ^{1}H NMR Spectrum of compound **6**

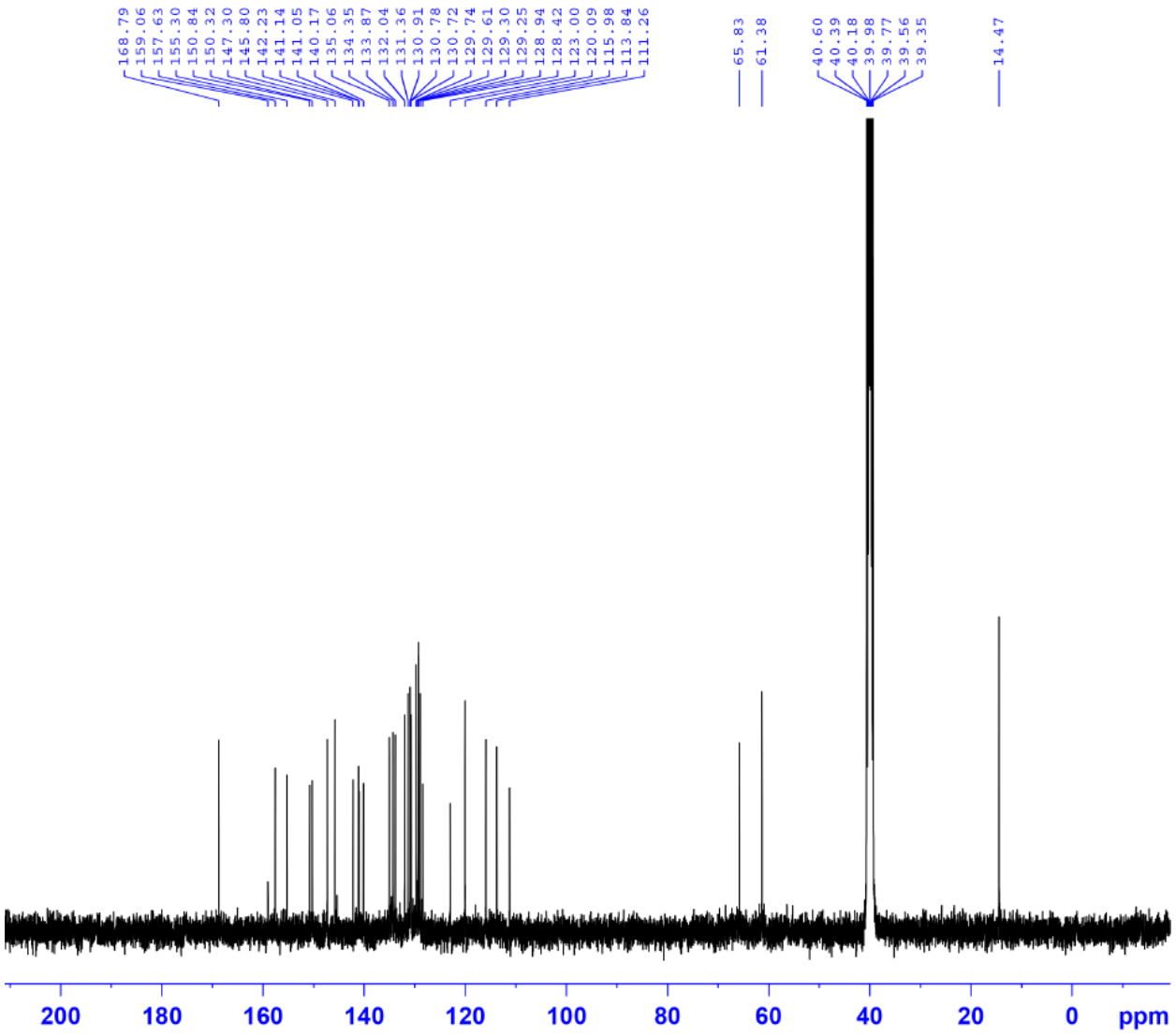

Figure 6b: ^{13}C NMR Spectrum of compound **6**

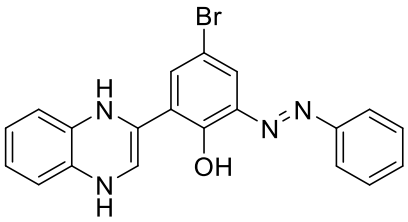

Compound **7**

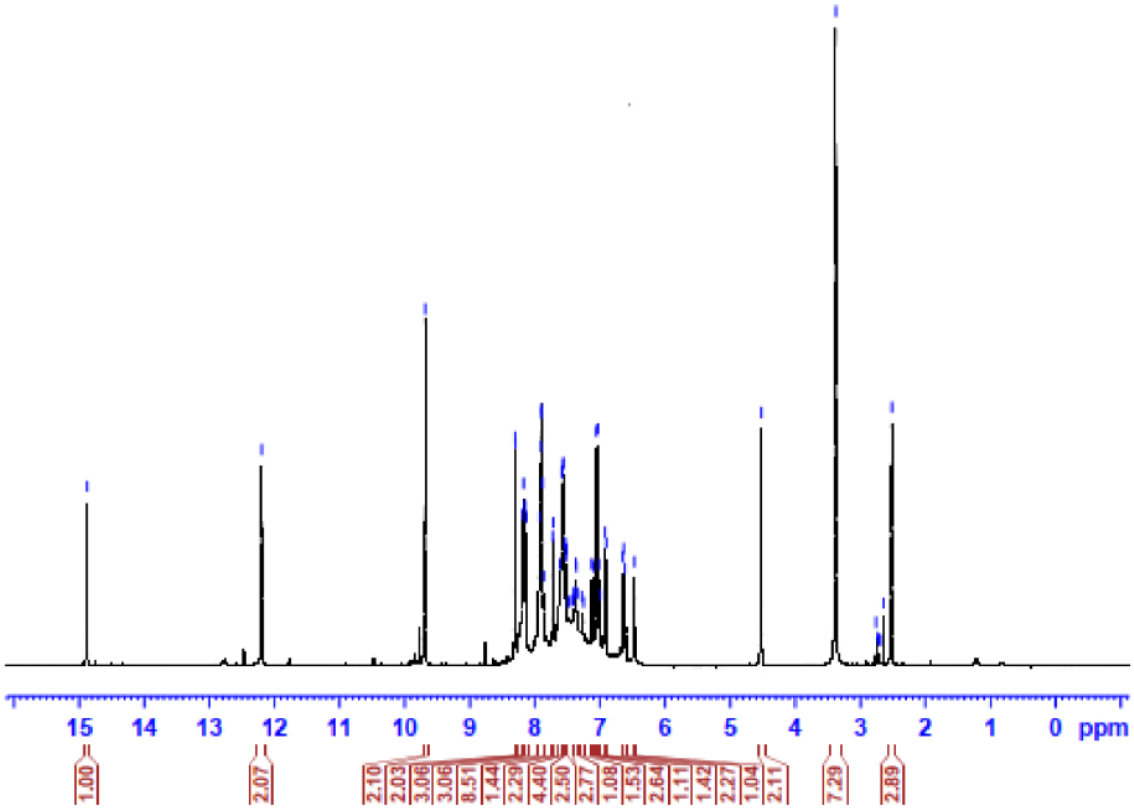

Figure 7a: ^{1}H NMR Spectrum of compound **7**

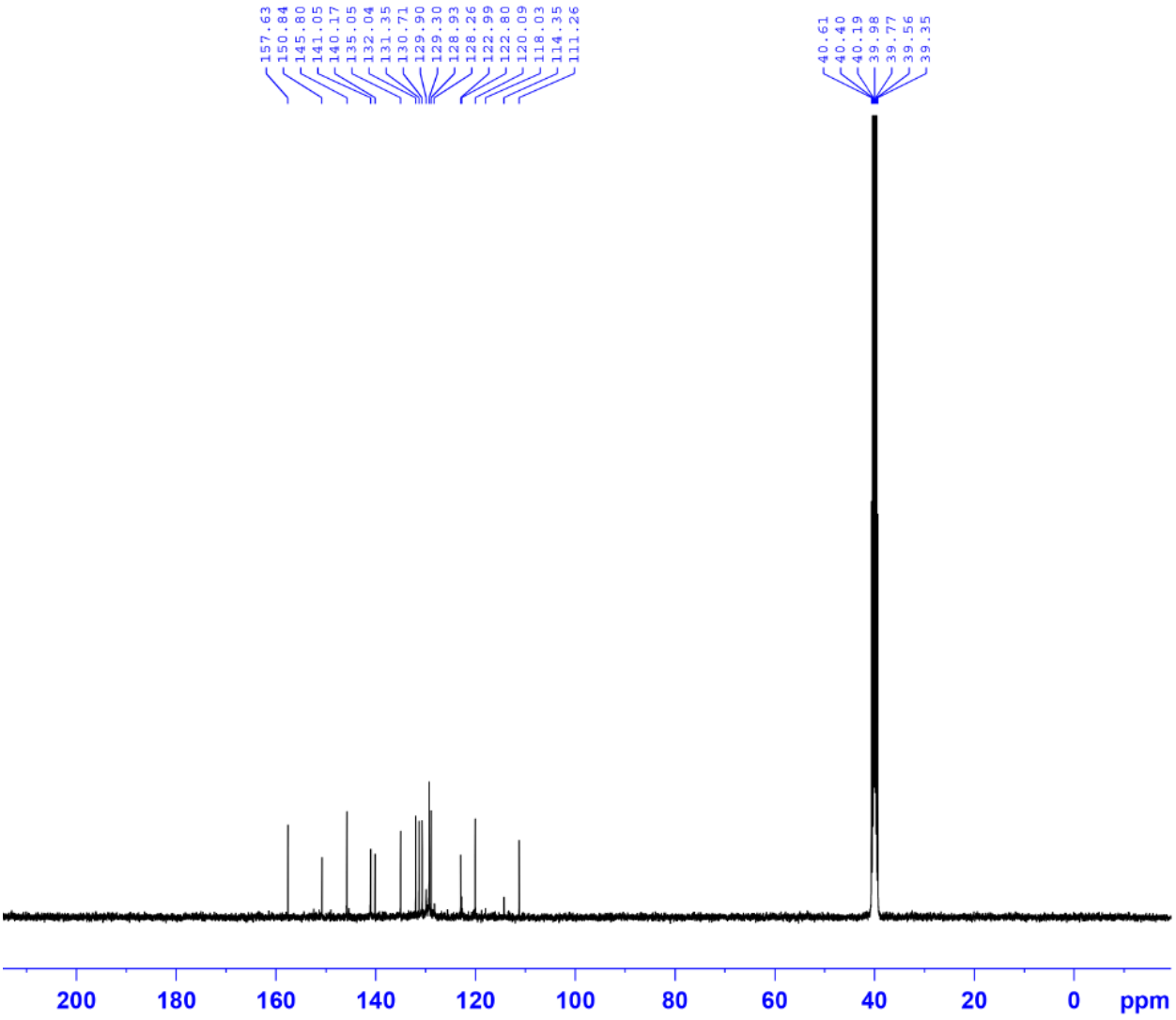

Figure 7b: ^{13}C NMR Spectrum of compound **7**

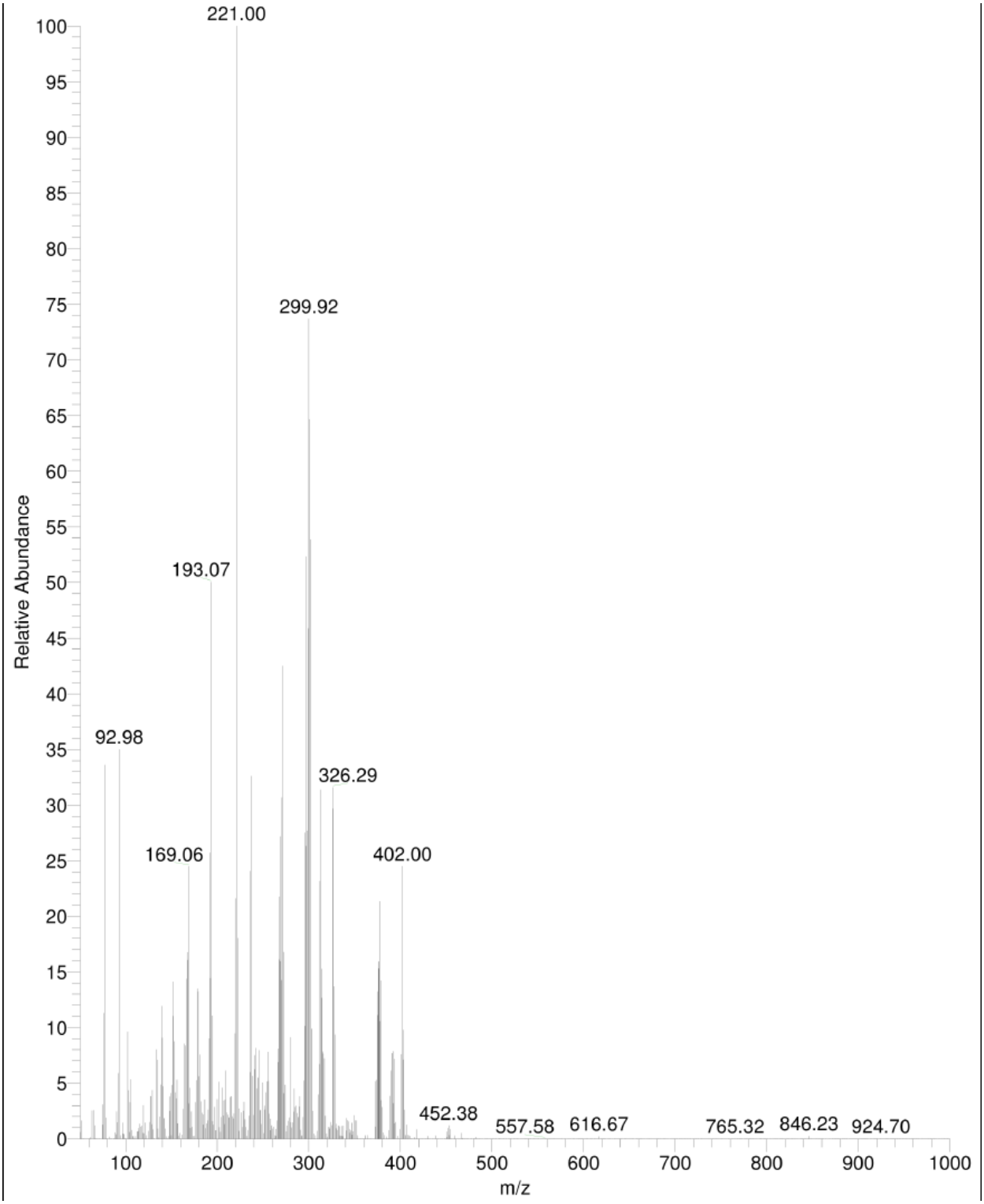

Figure 7c: Mass Spectrum of compound **7**

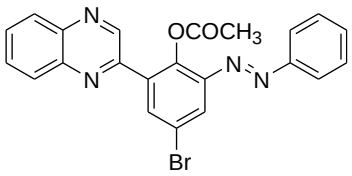

Compound **8**

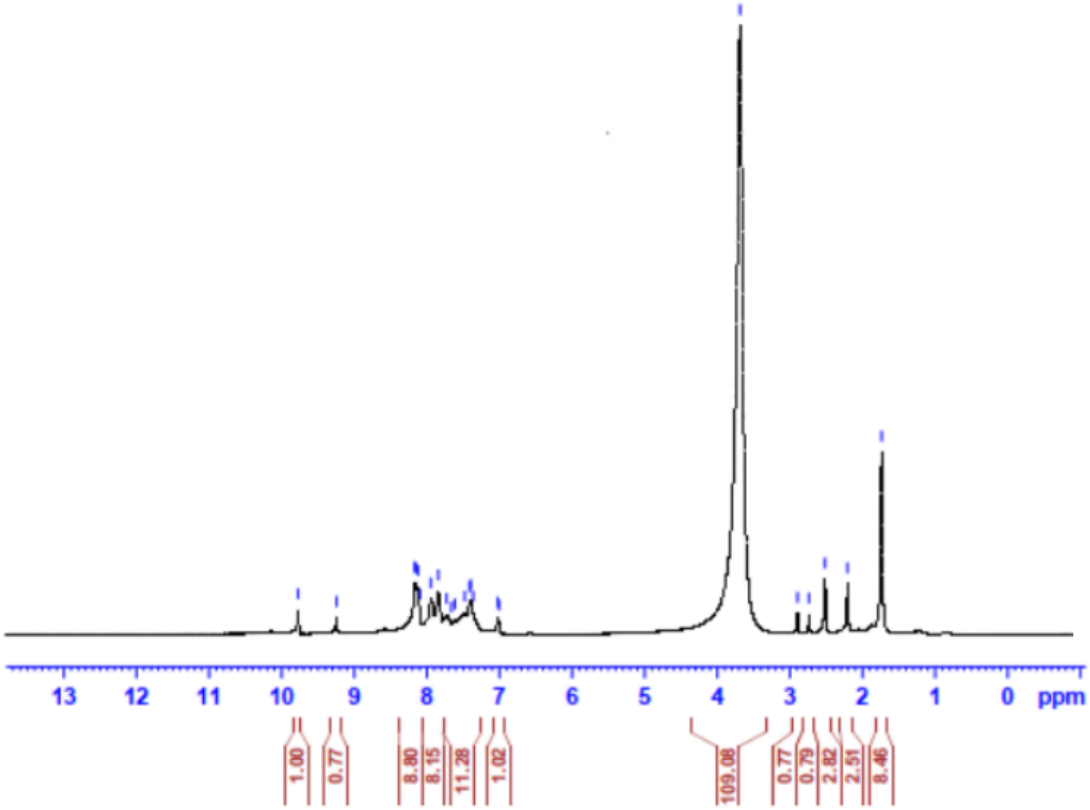

Figure 8a: ^{1}H NMR Spectrum of compound **8**

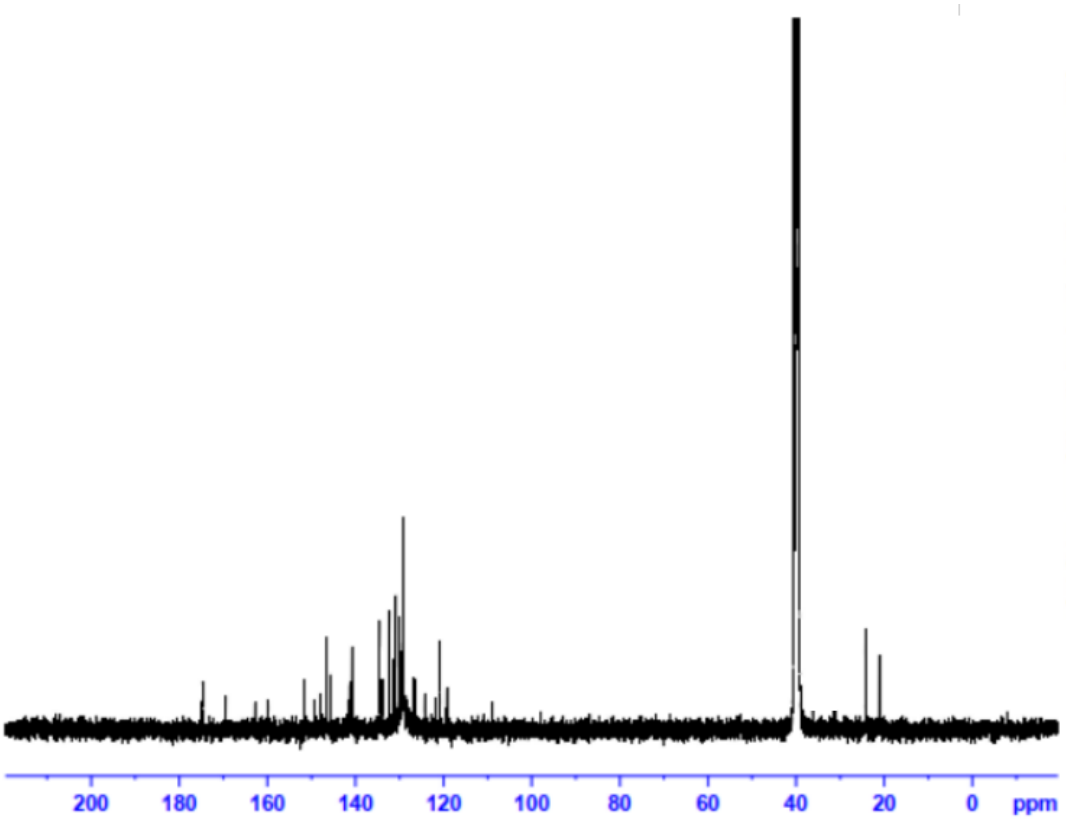

Figure 8b: ^{13}C-NMR spectrum of compound **8**

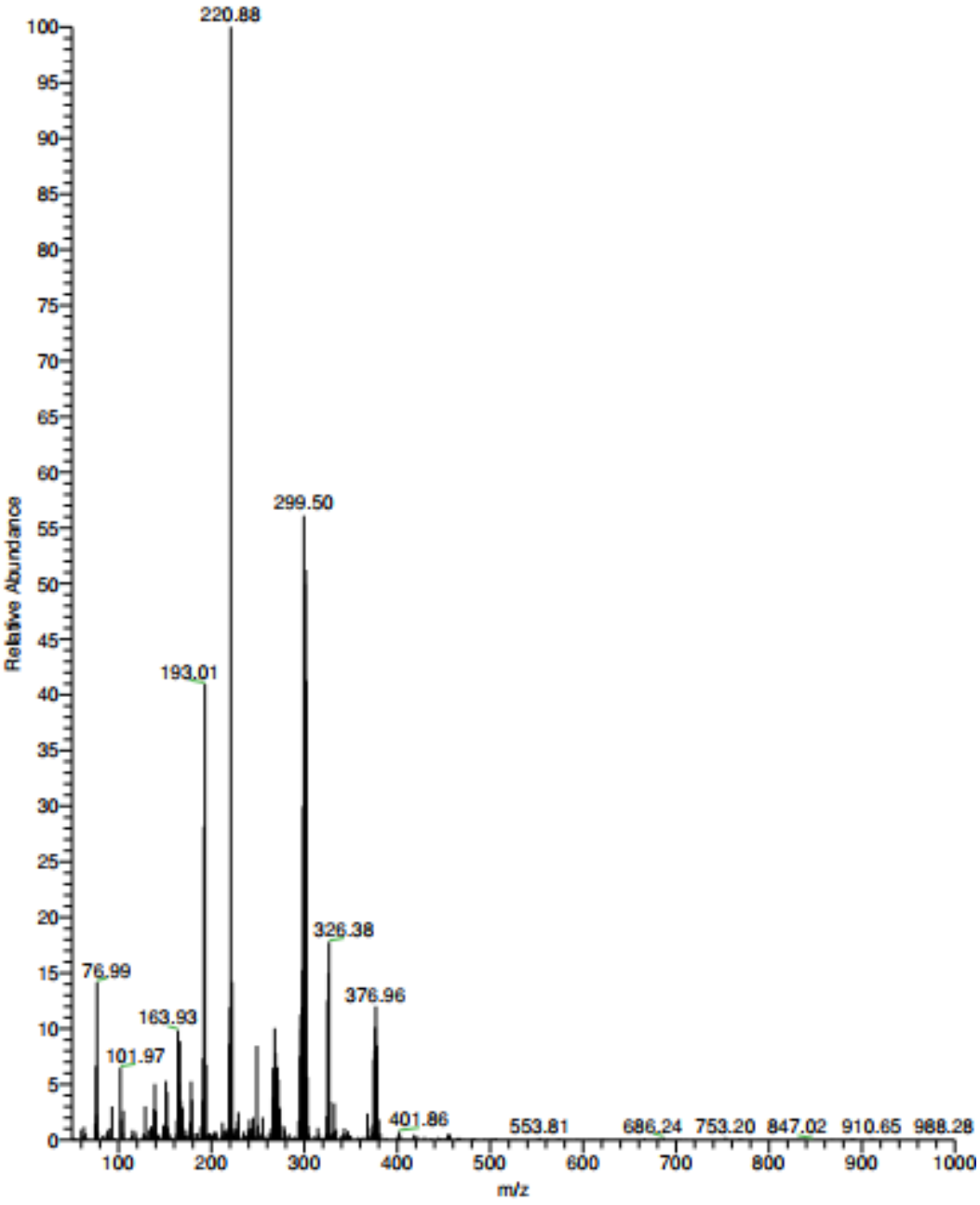

Figure 8c : Mass spectrum of compound **8**

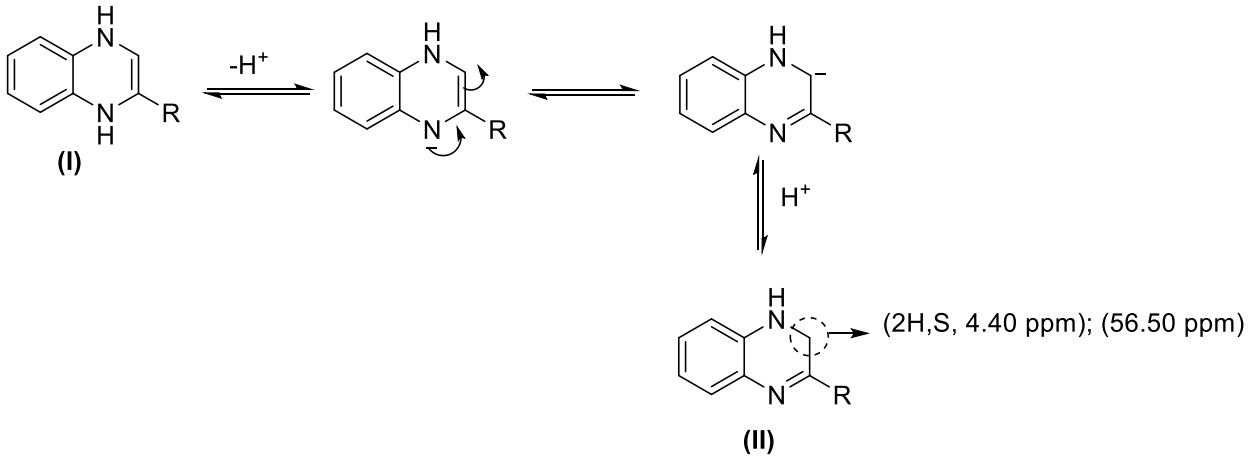

Figure S9: The suggested mechanism of 1,4-dihydroquinoxalin-1,2-dihydroquinoxalin isomerization.

***Molecular Docking Analysis* for 1,4-dihydro analogue**

Figure S10 depicts the overlay of the **3b** (1,4-dihydro isomer) with a docking score of -10.73 kcal/mol against EGFR target (PDB ID: *1M17*). This docked analogue, **3b**, engaged with specific amino acid residues like Met 742, Lys721, Thr830, Val702, Ala179, Thr766, Leu820, Met769, Leu694 and Pro770. Furthermore, the evaluation of the compounds' impact on inhibiting Human topoisomerase II (PDB ID: *5GWK*) was conducted, with **3b** (1,4-dihydro isomer) consistently emerging as the top docked candidate (among rest), achieving a docking score of -12.49 kcal/mol. The alignment of the best docked **3b** is depicted in **Figure S11**. Remarkably, **3b** (1,4 di-hydro isomer) maintained a notably lesser docking score of -12.49 kcal/mol in contrast to the 1,2-dihydro isomer of **3b** score of -13.72 kcal/mol. These findings strongly suggest the potential of compound **3b** 1,2-dihydro isomer as an inhibitor for both EGFR and Human topoisomerase II, underscoring the need for further exploration through in-vitro experiments.

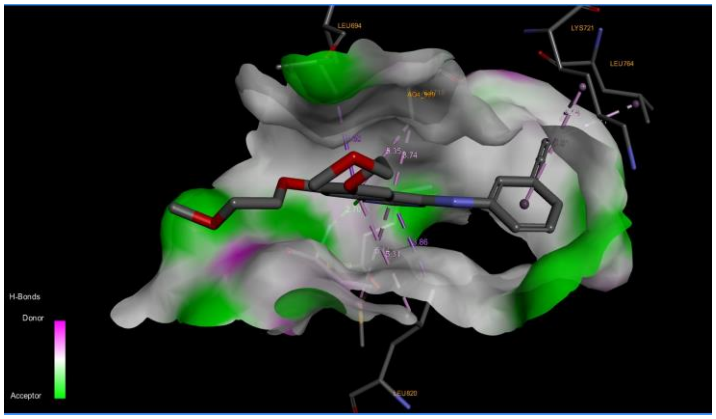

(A)

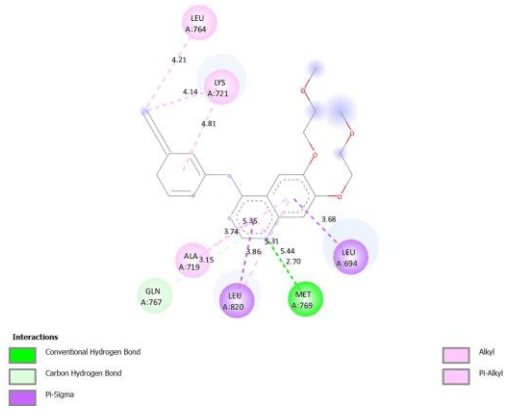

(B)

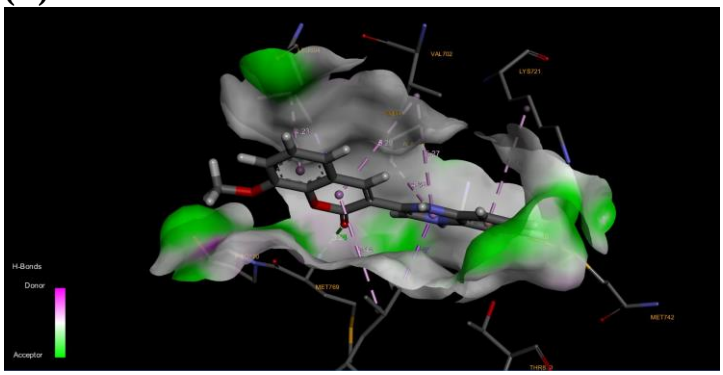

(C)

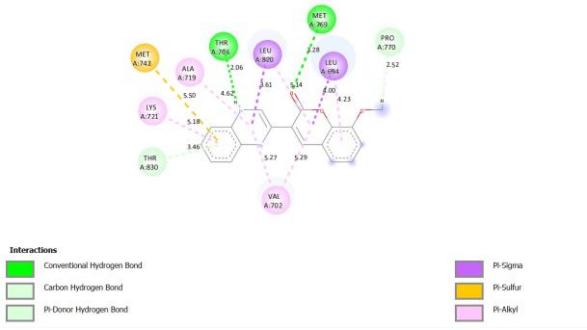

(D)

Figure S10. Descriptive 2D and 3D binding modes* of AQ4, co-crystallized ligand (**A, B**) and compound **3b (1,4-isomer)** (**C, D**) inside the pocket of the kinase domain from the epidermal growth factor receptor (EGFRK) (PDB code: *1M17*). *This figure was created by using Discovery Studio 4.0 Client (https://discover.3ds.com/discovery-studio-visualizer-download).

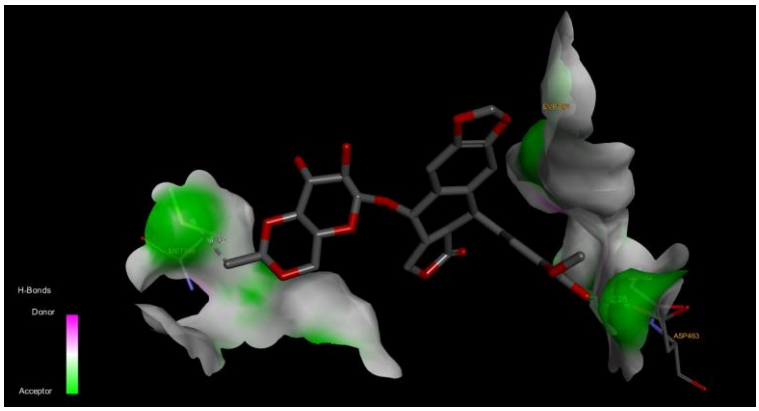

(A)

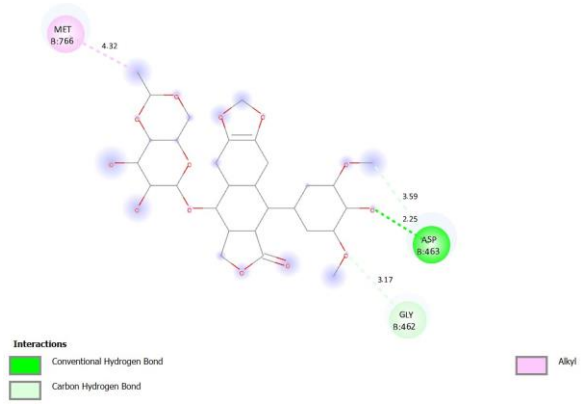

(B)

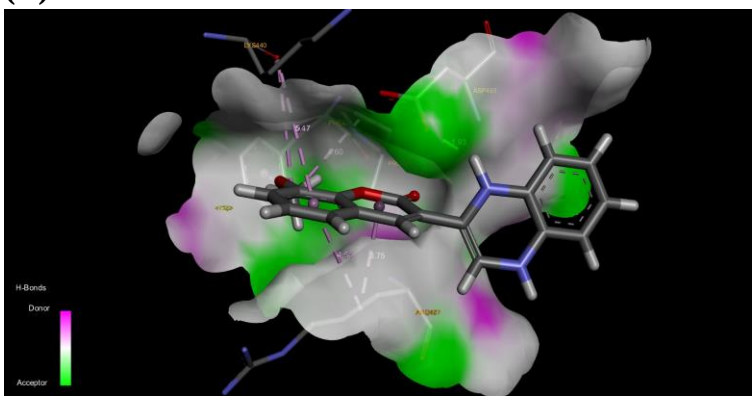

(C)

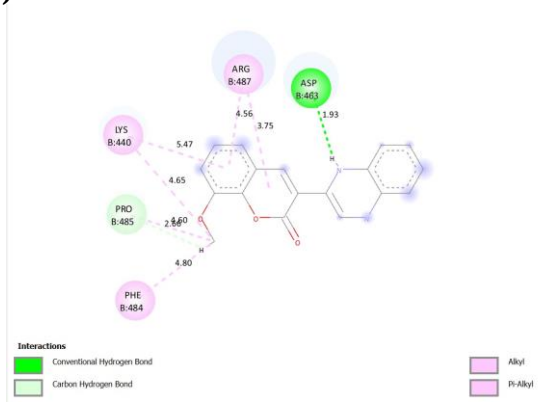

(D)

Figure S11. Descriptive 2D and 3D binding modes* of EVP, co-crystallized ligand (**A, B**) and compound **3b (1,4-isomer)** (**C, D**) inside the pocket of the kinase domain from Topoisomerase II (PDB code: *5GWK*). *This figure was created by using Discovery Studio 4.0 Client (https://discover.3ds.com/discovery-studio-visualizer-download).

Molecular Dynamics (MD) Analysis

The molecular dynamics simulations (MD) were employed to evaluate the stability of the top docked ligand, **1M17_3b** (1,4-dihydro) (least scored isomer), in relation to the target. This analysis was conducted over a 150 ns simulation duration using the software 'Desmond' by Schrödinger, LLC, New York, 2023. The comprehensive MD system comprised 34,246 atoms, including 9,896 water molecules, as illustrated in **Figure S12 (a-f)**.

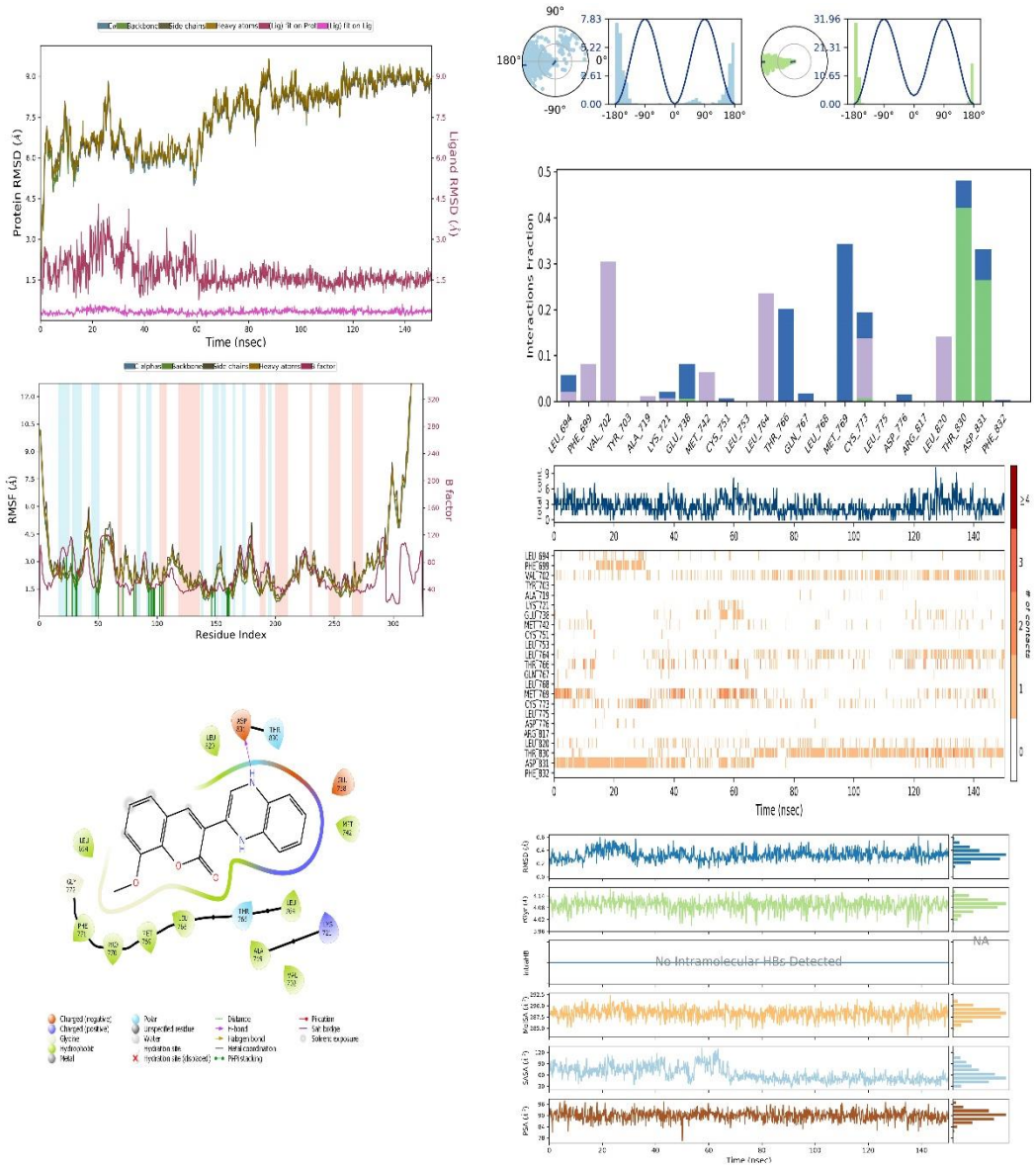

Figure S12. MD simulation analysis for complex **1M17_3b** (1,4-dihydro) (least scored isomer) (a) RMSD plot; (b) RMSF analysis; (c) Ligand-Protein contact plot; (d) Ligand torsion profile; (e) Protein-Ligand interaction plot; and (f) a timeline representation plot representing such interactions with amino acid residues over the simulation period of 150 ns.

In these simulations, we gauged the average displacements of atoms relative to a specific timeframe using the 'RMSD' (Root Mean Square Deviation) parameter. Our examination of the RMSD parameter disclosed a consistently stable conformation. When the ligand **3b** (1,4-dihydro) (least scored isomer) was bound to the target 1M17, the Cα-RMSD backbone RMSD values were consistently under 9.0 Å, and 'Lig_fit_Prot' values were maintained below 3.0 Å, as depicted in **Figure S12a**. Throughout the 0-150 ns period, the entire complex exhibited enduring stability. Moreover, localized fluctuations within the protein chains were scrutinized through the 'RMSF' (Root Mean Square Fluctuation) plot, detailed in **Figure S12b**. While there were minor spikes in fluctuation for specific amino acids, these variations didn't lead to significant changes, indicating their inherent flexibility. The analysis of the 'protein-ligand' interaction plot (**Figure S12c**) revealed crucial interactions, including hydrophobic interactions with amino acids Leu 694, Phe 699, Lys 721, Met 742, Leu 764, Cys 773, and Leu 820. No ionic interactions were observed, but there were hydrogen bonds with Thr 830 and Asp 831, along with water bridges involving residues like Lys 721, Leu 694, Glu 738, Thr 776, Gln 767, Met 769, Thr 830, and Phe 832. **Figure S12f** presented a timeline representation of these interactions with amino acid residues throughout the 150 ns simulation period. In **Figure S12e**, the 'ligand-protein' contact plot highlighted interactions occurring more than 5.0% of the simulation within the chosen trajectory (0.00 - 150.00 nsec). The 'ligand torsions plot' (**Figure S12d**) summarized the conformational changes of each rotatable bond (RB) in the ligand during the simulation trajectory (0.00 - 150.00 nsec). In summary, the ligand-protein conformation remained stable throughout the 150 ns simulation period. Thus, our docking analysis and molecular dynamics (higher values of RMSD and RMSF indicate larger fluctuations) pointed out the higher affinity of 1,2-dihydro analogue towards chosen targets. However, both isomers had minor differences in binding scores.